Molecular Dynamics Study of a MARTINI Coarse-Grained Polystyrene Brush in a Good Solvent: Structure and Dynamics

ARTICLE · JANUARY 2012

DOI: 10.1021/ma201980k

4 AUTHORS, INCLUDING:

Giulia Rossi
Università degli Studi di Genova
55 PUBLICATIONS **1,630** CITATIONS
SEE PROFILE

Tapio Ala-Nissila
Aalto University
360 PUBLICATIONS **5,035** CITATIONS
SEE PROFILE

Roland Faller
University of California, Davis
161 PUBLICATIONS **2,654** CITATIONS
SEE PROFILE

Macromolecules

ARTICLE

pubs.acs.org/Macromolecules

Molecular Dynamics Study of a MARTINI Coarse-Grained Polystyrene Brush in Good Solvent: Structure and Dynamics

Giulia Rossi,*[,†,⊥] Ian G. Elliott,[‡] Tapio Ala-Nissila,[†,§] and Roland Faller*[,‡]

[†]Department of Applied Physics, Aalto University School of Science, P.O. Box 11000, FI-00076 AALTO, Finland

[‡]Department of Chemical Engineering & Materials Science, University of California at Davis, One Shields Ave, Davis, California 95616, United States

[§]Department of Physics, Brown University, P.O. Box 1843, Providence, Rhode Island 02912-1843, United States

ABSTRACT: We use a newly developed model of polystyrene, based on the MARTINI coarse-grained force field, to study the behavior of polystyrene brushes in benzene via molecular dynamics simulations. We focus on chain lengths comparable to those accessible experimentally. We analyze the structural and dynamical configuration of the brushes as a function of their grafting density in a high grafting density regime (0.1−0.3 chains nm^{-2}). Only the highest density brush considered here (0.3 chains nm^{-2}) turns out to be characterized by a well-defined bulk area, where the density profile is flat, the lateral pressure profile has a plateau, and the chains are aligned perpendicularly to the substrate. At all grafting densities, our simulations reveal the presence of metastable collapsed states, with free chain ends trapped close to the substrate. These collapsed states are shown to be long-lived, surviving over a time scale of several microseconds.

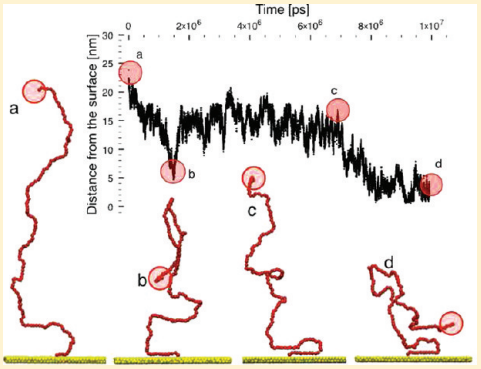

INTRODUCTION

Polymer brushes are abundantly used to tailor surfaces for specific applications .[1] Their main characteristics are the grafting density at the surface and the chain length. The recent development of accurate synthesis techniques, such as atom transfer radical polymerization, has led to the production of brushes with very high grafting density.[2,3] Regularly, the ratio between the gyration radius and the average distance between grafting points determines the various density regimes due to the degree of overlap of neighboring chains.[4] In the high-density regime, the distance between the grafted initiators on the substrate is significantly smaller than the average size of the free chain, causing the stretching of the brush in the direction perpendicular to the surface. High-density brushes are interesting for lubricant applications, thanks to their reduced friction coefficients.[5] Recently, new applications, far from the more traditional tribology area, have been explored. For example, the combination of high grafting densities and chain-end-functionalized brushes has revealed as a promising route for the patterning of biomolecules and inorganic particles, which can selectively bind on top of the substrate areas covered with the functionalized brush.[6,7]

The rational design of interface- or surface-active polymer modifiers still lacks crucial molecular scale information about the behavior and structure−property relationships of the brushes. This is especially true in the regime of dense brushes. However, such high grafting densities are potentially outside of the limits of classical polymer brush theory. Therefore, molecular modeling has to be applied to gain a theoretical understanding especially at the molecular level.

Polymeric systems are an inherent multiscale problem. This mandates the use of adapted molecular models. A few studies in atomistic detail have appeared, but they focused on short oligomer-like chains and/or low grafting densities.[8−10] On the other hand, polymer brushes have abundantly been studied by bead−spring type models[11,12] where the chemical specificity is lost. Such models are very valuable for understanding general dependencies on grafting density or chain length. But for direct comparison to experimental data more specific models are needed. Thus, between the all-atom and the bead−spring model a number of mesoscale models have been developed. For example, the iterative Boltzmann inversion has been used to develop intermediate scale specific models which have been used for the study of brushes.[13,14]

A promising alternative route to coarse-grained molecular modeling is given by the MARTINI model. MARTINI has been originally developed for lipids and other molecules of biological interest.[15−21] Recently, the MARTINI model has been extended to polymers such as polystyrene,[22] poly(ethylene oxide) and poly(ethylene glycol),[23] polyamido amine dendrimers,[24] and others.[25−28] In this paper we present the first application of the coarse-grained MARTINI model of polystyrene to the study of a highly dense polymer brush in a good solvent environment by means of molecular dynamics (MD) simulations. We analyze the structural and dynamical properties of the brush, with special focus on the trajectories of the chain ends which might eventually

Received: August 30, 2011
Revised: November 11, 2011
Published: December 08, 2011

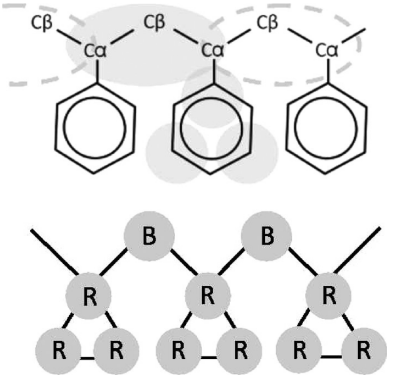

Figure 1. In the top image, gray areas on top of the atomistic description represent CG beads. In the CG molecule, at the bottom, backbone and ring beads are called B and R beads, respectively.

Table 1. Parameters of Bonded Interactions[a]

bond	r_{eq}	k_b	angle	θ_{eq}	k_a
B−R	0.27	8000	B−R−B	52	550
R−R	0.27	constr	R−B−R	120	25
			B−R−R	136	100

[a] B and R indicate backbone and ring beads, respectively (see Figure 1). r_{eq} (nm) and k_b (kJ mol^{-1} nm^{-2}) are the equilibrium bond length and the elastic constant of the harmonic bond potential. Very narrow atomistic distributions led us to constrain R−R bonds. θ_{eq} (deg) and k_a (kJ mol^{-1} deg^{-2}) are the equilibrium angle and the elastic constant of the harmonic angle potentials.

be functionalized. We compare the outcomes of our simulations to those of previous computational studies of polymer brushes, based on chemically nonspecific coarse-grained models. Moreover, we present our data in light of the available experimental data, and we discuss to what extent our MARTINI model can constitute a bridge between the predictions of the chemically nonspecific models and the experimental evidence related to the specific case of polystyrene.

In the section Model and Methods we describe our coarse-grained model of polystyrene, the brush setup, and the computational methods. The Results section contains the results of the structural and dynamical characterization of the brushes as a function of their grafting density. A discussion of the results follows in the Discussion section.

MODEL AND METHODS

Coarse-Grained Model of Polystyrene. We describe polystyrene chains by means of the MARTINI-based coarse-grained (CG) model we recently developed and validated.[22] Figure 1 shows how we mapped the atomistic description of polystyrene into the coarse-grained one. Each monomer is composed of four coarse-grained beads. Each bead represents two C atoms and their hydrogens. This relatively fine degree of coarse-graining allows for retaining the backbone−ring structure of polystyrene, and it is consistent with the 2-to-1 mapping scheme[16] of the MARTINI force field.

Bonds between CG beads are described by harmonic functions. We tuned their equilibrium values and force constants to reproduce at best the peak position and width of their atomistic

Table 2. Optimized Values of ε and σ Lennard-Jones Parameters for the MARTINI PS Model[a]

parameter	σ_{B-B} [nm]	ε_{B-B} [kJ/mol]	σ_{B-R} [nm]	ε_{B-R} [kJ/mol]	σ_{R-R} [nm]	ε_{R-R} [kJ/mol]
PS model	0.43	2.625	0.43	2.325	0.41	2.4

[a] B and R subscripts stand for backbone and ring, respectively.

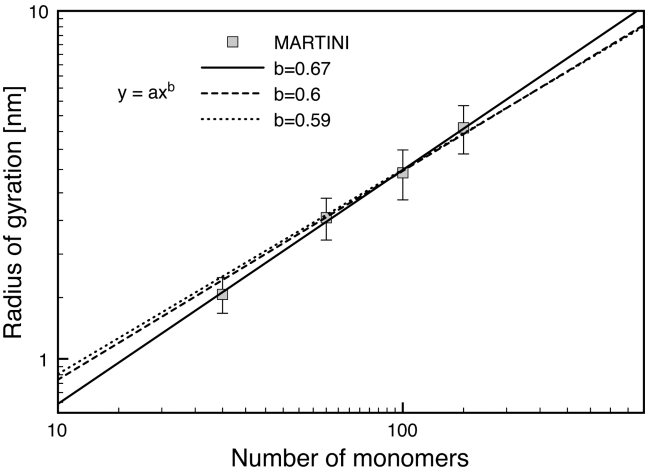

Figure 2. Radius of gyration of polystyrene in benzene solution. Squares are for the simulation data, the continuous line is the best fit to a power law function $y = ax^b$, and the dotted and dashed lines are the best fit to a power law function with exponent $b = 0.588$ and $b = 0.6$, respectively.

counterparts.[22] The model does not include any torsional angle at coarse-grained level. Parameters for the harmonic bonded interactions of the model are reported in Table 1.

In MARTINI, nonbonded interactions between noncharged beads are described by Lennard-Jones potentials. The MARTINI force field includes a large number of beads, each describing a chemical building block characterized by a specific degree of polarity. Lennard-Jones interactions of MARTINI beads are assigned to reproduce experimental thermodynamic data, such as densities and free energies of transfer between water and oil. In our model, the parametrization of polystyrene resulted from a refinement of the original MARTINI parametrization. The refinement aimed at a faithful reproduction of the density and radius of gyration of polystyrene in the melt.[22] Optimized values for the interactions between B (backbone) and R (ring) beads are reported in Table 2, while more details about the parametrization procedure can be found in ref 22.

MARTINI Polystyrene in Benzene. For polystyrene in dilute conditions, the force-field parameters in three different solvents (benzene, cyclohexane, and water) were derived earlier[22] and are available on line.[29] Here we need to describe polystyrene brushes in good solvent conditions, and thus we will solvate the PS brushes in benzene. Within the MARTINI scheme, each benzene molecule is represented by three interconnected beads (MARTINI type SC4). The parameters for the interaction between the PS backbone beads and the MARTINI benzene beads are the same as for the SC1−SC4 interaction in the original MARTINI parametrization,[16] while the interaction between PS ring beads and benzene beads uses the SC4−SC4 interaction.

dx.doi.org/10.1021/ma201980k |Macromolecules 2012, 45, 563–571

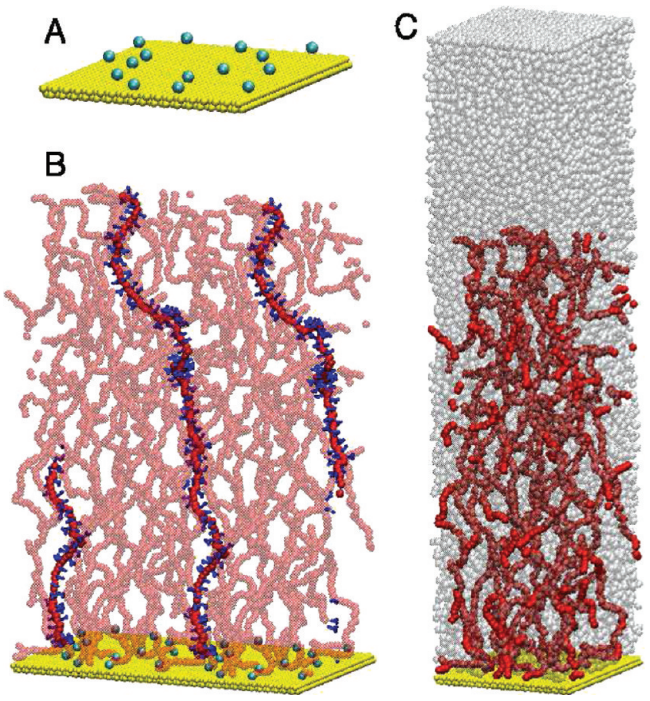

Figure 3. Snapshots from the equilibration runs of the 15 chain system. (A) The 2450 particle substrate and the grafted backbone beads. (B) Two periodic images of the substrate, the grafted beads, and the PS chain backbones. For one of the chains, extending through the box boundaries, we show both backbone beads (red, large) and phenyl rings (small, dark triangles). (C) The substrate, the PS backbones (red), and the benzene solvent (transparent gray).

We verified the reliability of the model by simulations in the *NpT* ensemble of single PS chains of 30, 60, 100, and 150 monomers in benzene at 300 K and 1 bar. The edges of the cubic simulation box varied from 5.8 nm (PS30) to 8.8 nm (PS150) to exclude the interaction of the PS chain with itself, and the runs were 2 μs (PS30), 3.5 μs (PS60), and 5 μs (PS100 and PS150) long. Figure 2 shows the average values of the radius of gyration vs chain length, together with three fitting power law functions. The best fit is given by a scaling exponent of 0.67, while the 0.588 predicted by Flory's theory[30] and the 0.6 value reported experimentally[31] lie within the statistical error bars.

Polystyrene Brushes. Our brushes consist of polystyrene chains of N = 150 monomers grafted to a solid substrate in benzene solution. The substrate consists of two (111) layers of particles (MARTINI type C4), with lattice constant l = 0.25 nm and normal vector along the z direction. The substrate particles have a nonpolar character, and the strength of their interactions with the PS and benzene beads is in the same range as the PS−PS and PS−benzene interactions, namely between 3.1 and 3.5 kJ/mol.[22] The substrate area, A, is 8.7 × 7.4 nm. Substrate beads are restrained to their initial lattice positions by means of a spherical harmonic potential with elastic constant k_{sub} = 8000 kJ mol^{-1} nm^{-2}.

In order to mimic the presence of a covalent bond connecting the chain ends to the substrate, we have restrained the position of the first backbone bead of each PS chain to a random (x,y) position, at a fixed distance from the substrate, z_{bb} = 0.3 nm. The restraining of chain ends is realized with the same harmonic potential used for the substrate beads. We consider three different grafting densities: 0.15, 0.23, and 0.31 chains nm^{-2}

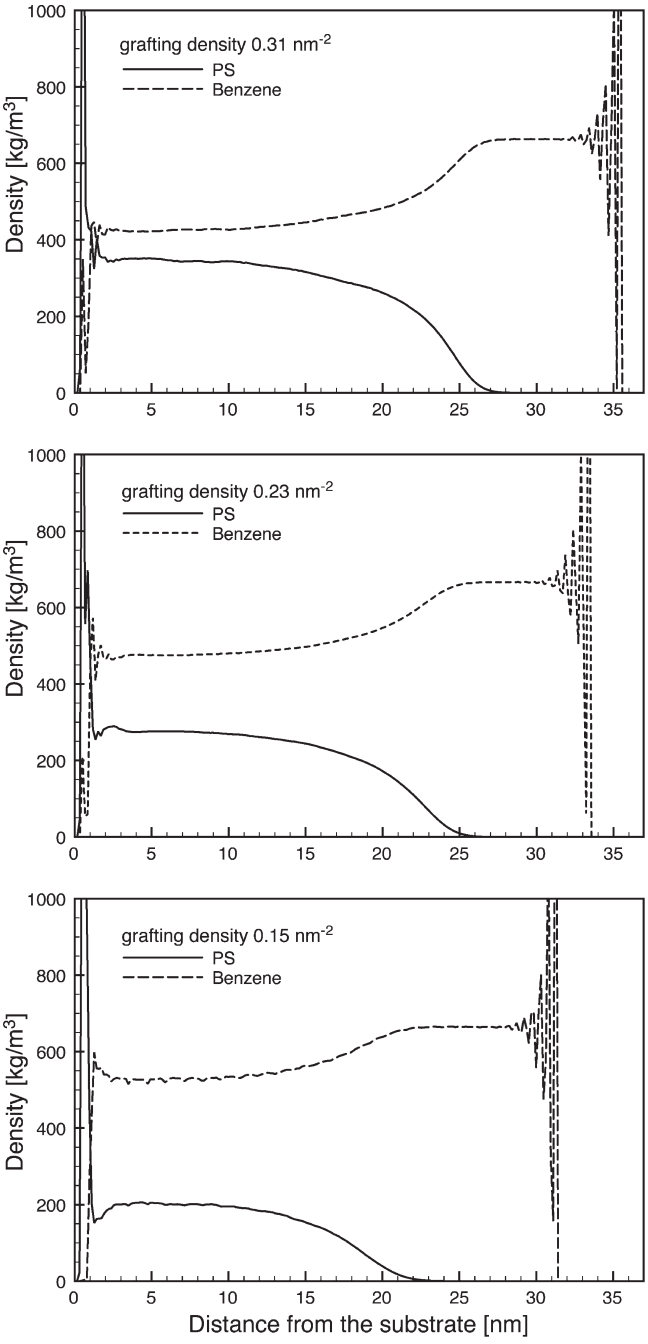

Figure 4. Density profiles of the brushes. Density values have been rescaled converting MARTINI masses[16] to atomistic masses.

(corresponding to 10, 15, and 20 chains in the simulation box). We are thus focusing on a rather high-density brush regime, our density values being comparable to those used in previous computational[10,32] and experimental[3,33] works. However, in contrast to earlier simulations our brushes are longer.

Simulation Protocols. *Brush Preparation and Equilibration.* All molecular dynamics simulations were run with the GROMACS package,[34] version 4.0.7. Brushes were built up in three steps: (a) We assigned random (x,y) coordinates, at distance z_{bb} from the substrate, to the first backbone bead of each chain. The distance between grafting points on the (x,y) plane was set to be larger than 1 nm, to avoid an uneven distribution of the chains on

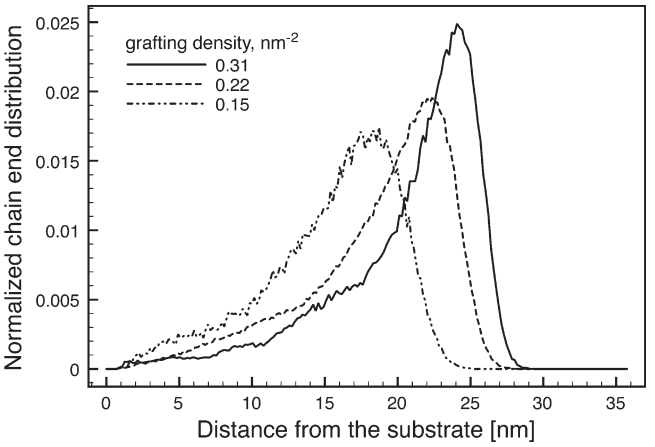

Figure 5. Normalized chain end distribution along the direction perpendicular to the substrate.

the substrate. (b) We grew fully stretched brushes starting from the grafted backbone beads, and benzene molecules were added all over the simulation box, avoiding overlap and interpenetration of ring structures. (c) We equilibrated the system. We used periodic boundary conditions in all directions. Temperature was controlled by a Berendsen thermostat[35] at 400 K. We applied Berendsen pressure coupling[35] (reference value 1 bar) along the z direction and set the system compressibility to 0 along the x and y directions to achieve a NAP_zT ensemble. As a criterion to stop the equilibration procedure, we waited for the brush and solvent density profiles to converge, which typically happened on a microsecond time scale. As a result of the equilibration, the z dimension of the simulation box measured 31−36 nm, including a thick (>8 nm) benzene layer at the top of the brush.

Production Runs. We generated, as detailed above, one starting configuration for the 20-chain system and three independent starting configurations for both the 15- and 10-chain systems. We performed the production runs at the constant temperature of 400 K, controlled by a Nosé-Hoover thermostat.[36,37] A semi-isotropic pressure coupling was applied, keeping the x and y dimensions fixed and allowing for the relaxation of the z dimension of the simulation box using a Parrinello−Rahman barostat.[38,39] We used a time step of 20 fs, and the duration of each independent simulation was 10 μs, amounting to a total of 30, 30, and 10 μs for the 10-, 15-, and 20-chain systems, respectively.

RESULTS

Structure. *Density Profiles.* Figure 4 shows the density profiles of the brushes at equilibrium. In MARTINI, all CG beads are given the same mass, and data here have been rescaled to atomistic density values. The density profiles at the top of the simulation box exhibit sharp peaks that reveal the tendency of the solvent to form 2D liquid layers as getting close to the upper periodic image of the substrate. This is a well-known effect,[40] explained in terms of solvation forces and frequently observed in simulations of Lennard-Jones liquids in contact with solid surfaces.[11,41] At the bottom of the brush, such a layering effect superposes to a large density peak of polystyrene. The peak is due to the flattening against the solid surface of the first monomers of some polymer chains. From an enthalpic point of view, the attraction between the solid surface and polystyrene beads is not

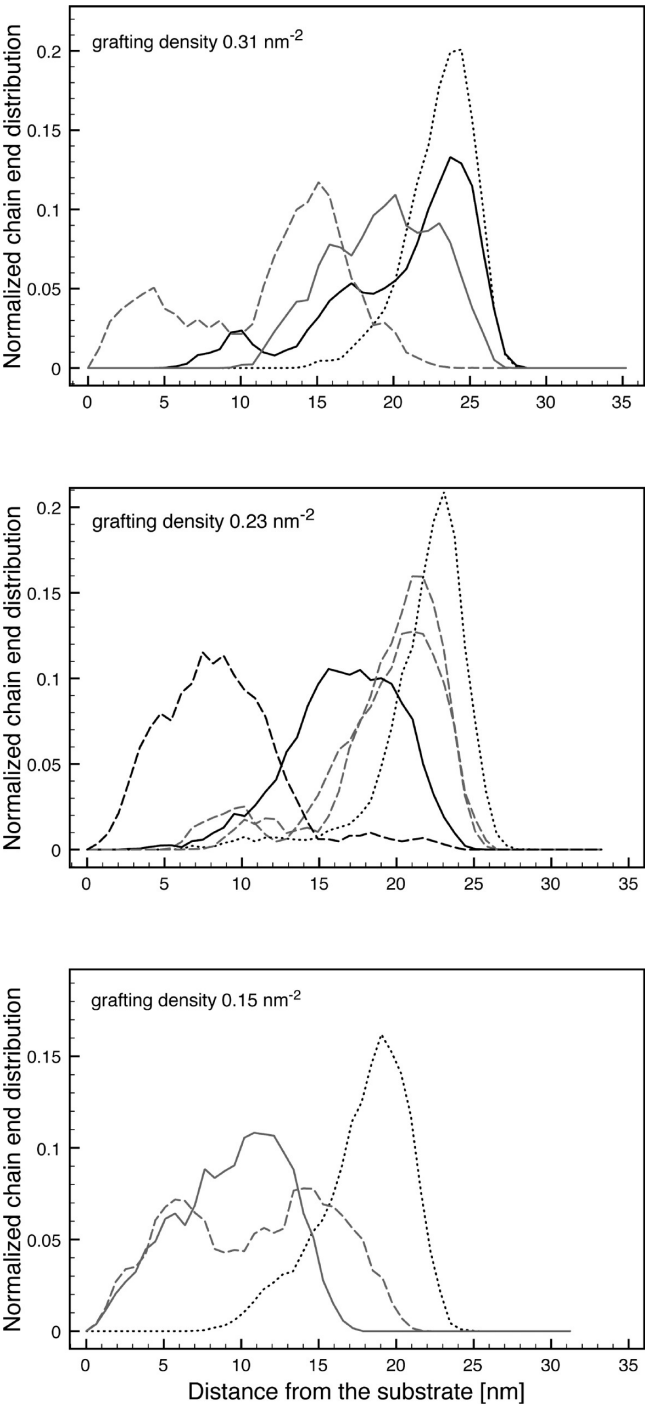

Figure 6. Normalized chain end distribution along z. Here, only some of the end chain distributions are shown for each grafting density. Top: at the highest grafting density, one trimodal distribution is observed (black, thick line), several bimodal distributions (one example shown with dashed gray line), and single-peak distributions with different broadness (thick gray line and black dotted line). Middle: at the intermediate grafting density, bimodal distributions (dashed gray lines) and single-peak distributions of different broadness are observed (black dashed, black thick, black dotted lines). Bottom: for the lowest grafting density, only a very few bimodal distributions are observed (gray dashed line), while all the other distributions are single-peak distributions, with different broadness.

stronger than between the solid surface and benzene. The preference for adsorbing fragments of polymer chains rather

dx.doi.org/10.1021/ma201980k |*Macromolecules* 2012, 45, 563–571

Table 3. Percentages of Chains Whose z Chain End Distribution Is Single-Peak, Bimodal, or Trimodal[a]

	single-peak [%]	bimodal [%]	trimodal [%]
0.3 nm^{-2}	45	20	5
0.23 nm^{-2}	66	15	0
0.15 nm^{-2}	73	13	0

[a] Total number of chains, each analyzed over a 10 μs run, is 20, 45, and 30 for the largest, intermediate, and lowest grafting density considered, respectively.

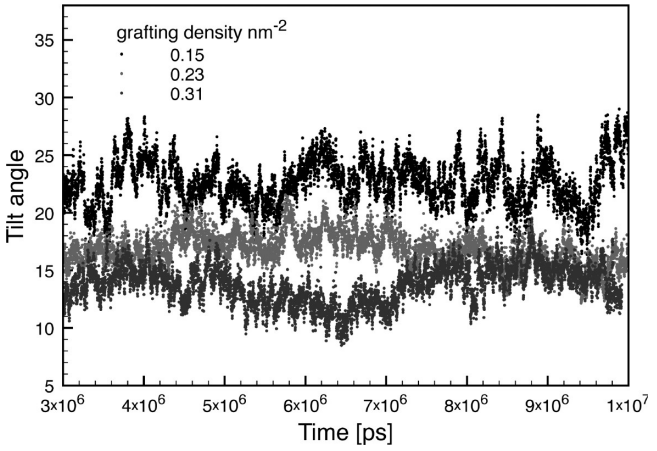

Figure 7. Tilt angles.

than solvent molecules has been observed in other molecular dynamics simulations of polymer brushes, with a more coarsened description of solvent and polymer chains.[32] We thus attribute the preference for PS adsorption at the surface to entropic forces. Our brush density profiles appear to be rather flat along the first third of the brush height and then start to decrease smoothly. Thus, we do not observe a fully parabolic profile for the whole brush but find a plateau which is only observed in very high-density systems.[32,42,43]

Distribution of Chain Ends. We define as z profile, $P(z)$, the normalized distribution of the z coordinate of the free chain ends of the brush. Figure 5 shows the average z profiles we obtained at the different grafting densities. The profiles reveal a strong stretching regime[42] for all the grafting densities considered. While the peak of the distribution moves far from the surface as the grafting density increases, the shape of the distribution changes as well. The relative fluctuation of the distance z between the chain ends and the substrate, namely $f = (\langle z^2\rangle - \langle z\rangle^2)^{1/2}/\langle z\rangle$, gets smaller as the grafting density increases: f = 0.29, 0.26, and 0.23 for brushes with 10, 15, and 20 chains, respectively.

The average chain end z profiles are characterized by small shoulder peaks around 15, 11, and 5 nm from the surface for the high, intermediate, and low grafting densities considered. In order to elucidate the nature of these secondary peaks, we analyzed the z profiles of the single chain ends. On the basis of the appearance of distinguished and significative peaks in the distributions, we classified them as trimodal, bimodal, and single-peak. Several examples are shown in Figure 6. Table 3 quantifies the percentual appearance of these three kinds of distributions as a function of the brush density. Clearly, single peak distributions

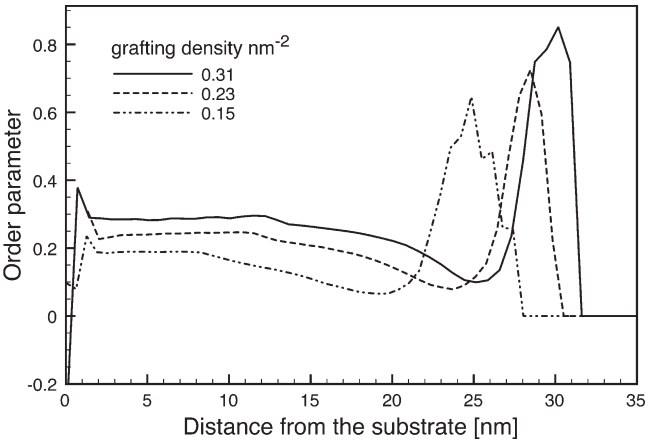

Figure 8. Order parameter $P_2(\theta)$ of backbone bonds as a function of their distance from the substrate.

become prevalent as the brush density decreases, at the expense of multimodal distributions.

Chain Tilt. We measured the tilt angle θ formed by the normal to the substrate plane and the vectors connecting each grafted backbone bead to its free chain end. θ is equal to zero when the chain end is placed right on top of the grafted bead and $\pi/2$ when it is in contact with the surface. Average values of the tilt angle for the brushes with 10, 15, and 20 chains are 22.8, 16.8, and 13.7. Fluctuations around average values are 0.16, 0.16, and 0.15, respectively. The chains become more perpendicular to the surface with increasing grafting density.

Single chain tilt angle distributions exhibit multimodal shapes, similar to those observed for the z chain end distributions. By analyzing the single chain tilt angles, we observed the penetration of chain ends deeply into the brush bulk, reaching tilt angles $\theta > \pi/3$. These events became increasing likely as the density of the brush decreased but were observed also for the highest grafting density considered here.

Bond Alignment with the Normal to the Surface. By increasing the grafting density, the chains stretch and the peak of the chain end distribution moves away from the grafting surface. The stretching is correlated to the alignment of the chain bonds to the normal to the grafting surface, as measured by the order parameter $P_2(\theta) = (3\langle\cos^2(\theta)\rangle - 1)/2$, θ being the angle formed between each chain bond and the normal. P_2 has the value $-1/2$, 0, and 1 for perpendicular, random, and parallel alignment to the normal, respectively. Dimitrov et al.[11] showed the dependence of the order parameter on the monomer index, finding progressive disalignment of the bonds with decreasing grafting density or quality of the solvent. Since the observation of single chain end distributions show that free chain ends can be found well deep into the brush bulk, in Figure 8 we plot the order parameter as a function of the distance from the grafting surface. The negative peak registered close to the surface has to be attributed to the flattening of the first monomers of the chains on top of the grafting surface. In the brush bulk, a flat region can be clearly identified for all the grafting densities considered. The larger the grafting density, the longer the plateau and the larger the degree of alignment. Interestingly, the order parameter highlights the large degree of alignment of the chain ends, in those rare cases when the chains get to be almost ideally stretched.

Pressure Profiles. We calculated the lateral pressure profile of the brush, defined as $\pi(z) = p_L(z) - p_{zz}(z)$, p_L being the average

between the in-plane diagonal components of the local pressure tensor, $p_L = (p_{xx} + pp_{xx})/2$. We performed the calculation of the local pressure tensor as in Ollila et al.[44] As shown in Figure 9, at all grafting densities, the lateral pressure profile is positive and does not show any negative peak at the top of the brush, as it would be expected in presence of a sharp polymer−solvent interface.[11] The profile of the brush with the highest grafting density shows a clear plateau region extending for 15 nm, followed by a progressive decrease which leads to a homogeneous pressure tensor (isotropic hydrostatic pressure) in the pure solvent region. At the lowest grafting density, no clear plateau can be identified,

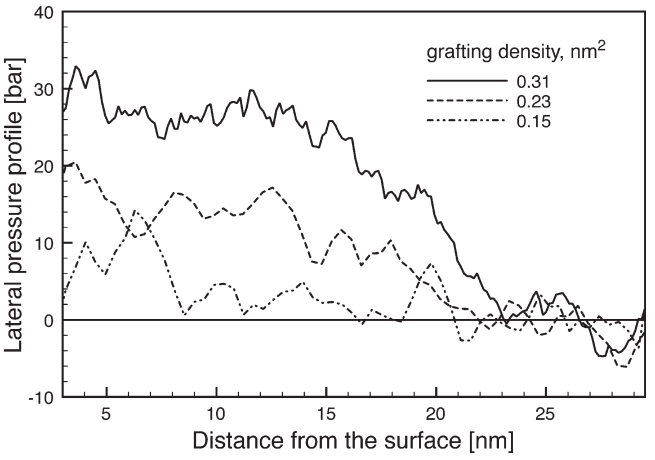

Figure 9. Pressure profile.

and in most of the brush thickness the difference between the perpendicular and parallel components of the stress tensor is negligible. The surface tension across the brush, namely $\gamma = -\int_0^{z_{max}} \pi(z)\, dz$ (z_{max} being placed in the homogeneous solvent region, where the lateral pressure profile vanishes), increases with increasing grafting density.

Dynamics. *Trapped States.* The single chain distributions of free chain ends and tilt angles suggest the possibility that some brush chains may get trapped in metastable states, characterized by large tilt angles and/or deep penetration of the chain ends into the brush, close to the grafting surface. We thus proceed to the analysis of the time-dependent single-chain behavior, with the aim to verify the existence of such trapped states and provide an estimate of their lifetime as a function of the grafting density.

To start with an example, we can focus on a chain whose z chain end distribution is bimodal, with both peaks lying below the brush surface, at 15 and 4 nm (as shown in the top panel of Figure 6). Figure 10 shows the z coordinate of the chain end plotted as a function of time. Starting from an extended state (a), the chain end initially collapses to low z (b) and then finds an intermediate state (c) for more than 5 μs. At the end of the simulation, the chain collapses again and the final state is observed over the last 2 μs of the simulation.

The relatively low number of chains sampled by our simulations does not allow for a quantitative estimate of the lifetime of the collapsed metastable states. Still, from the analysis of the z distribution of the chain ends, some qualitative conclusions can be drawn. The extended configurations show the longest lifetime and in several cases appear to be stable throughout the whole 10 μs run.

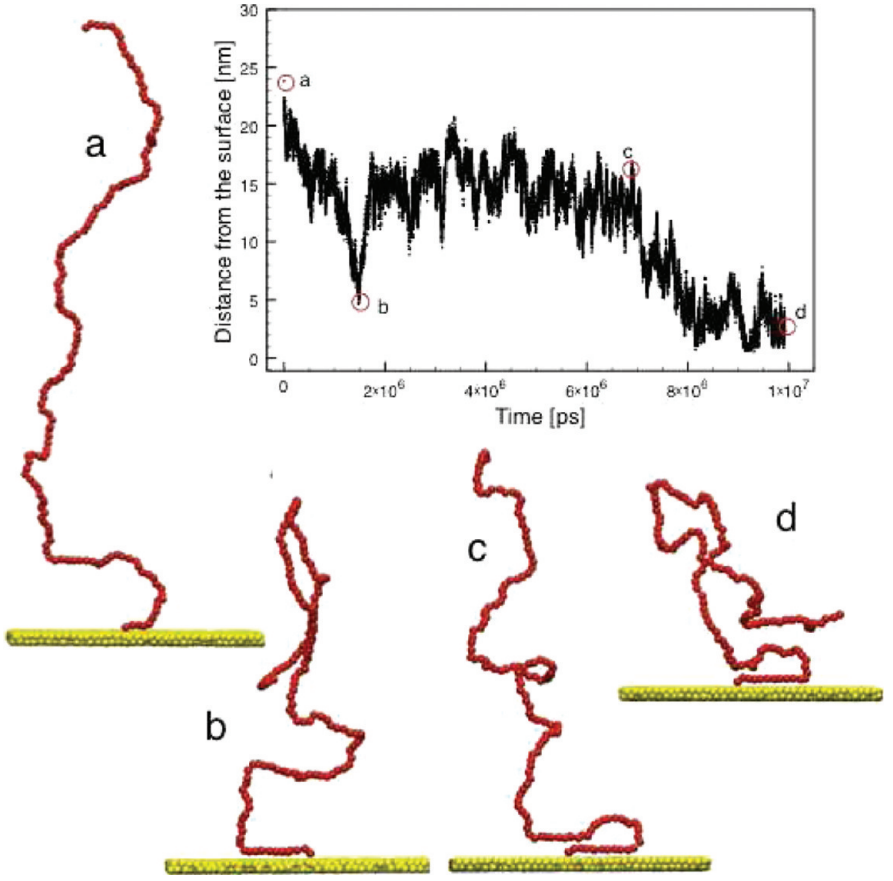

Figure 10. Extended and collapsed states for a chain at 0.31 nm^{-2} grafting density.

dx.doi.org/10.1021/ma201980k |*Macromolecules* 2012, 45, 563–571

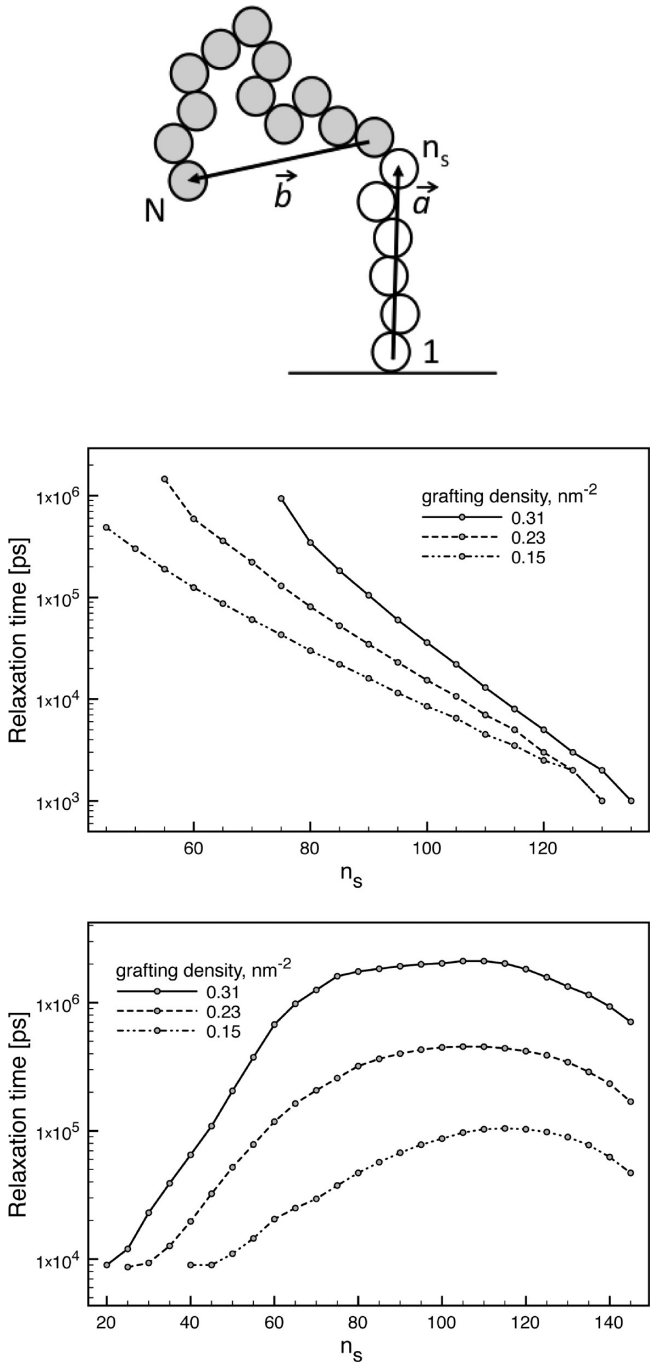

Figure 11. Top panel: the grafted, $\vec{a}$, and terminal, $\vec{b}$, segments of the chains used to calculate orientational relaxation times. Middle panel: relaxation times of the terminal segments, as a function of n_s. Right: relaxation times of the grafted segments. Lines are only guides for the eyes.

Collapsed configurations, with chain ends a few nanometers below the brush surface, have a lifetime of 2−5 μs. Collapsed states where the chain end is very close to the grafting surface survive for shorter times, ranging from a few hundreds of nanoseconds to a couple of microseconds. While clear transitions from extended to different collapsed configurations can be always be spotted for the high- and intermediate-density systems, at the lowest grafting density the transitions from extended to collapsed configurations becomes smoother, in agreement with the lower grafting density brushes completely consisting of one interface region.

Segmental Relaxation Times. The chains need to completely reorient their terminal segment in order to access the collapsed, trapped states described in the previous paragraph. As shown at the top of Figure 11, we can ideally split the chain in a grafted, presumably stiffer region, containing n_s monomers, and a mobile region, containing $n_m = N - n_s$ monomers. The vector $\vec{a}$ connects the first, grafted backbone bead of the chain to the bead at position n_s, while the vector $\vec{b}$ connects the bead at the position $n_s + 1$ with the chain end. The transition from the stretched configurations to the collapsed states described above implies the complete reorientation of long terminal segments ($n_s > 70$). Thus, we first look at the rotational autocorrelation function, $C_b(t)$, of $\vec{b}$, namely, the vector connecting the first of the mobile monomers to the free chain end. $C_b(t)$ is defined as $C_b(t) = \langle P_2[\hat{b}(t)\hat{b}(0)]\rangle$, P_2 being the second Legendre polynomial and $\hat{b}$ a unitary vector directed as $\vec{b}$. The smaller n_s, the slower the reorientation of our terminal segment. In order to be able to compare the behavior of terminal segments of different length, at different grafting densities, we define as relaxation time τ_r the time at which $C_b(t)$ reaches a value of 0.6. The middle panel of Figure 11 shows the average data obtained from our simulations at high, intermediate, and low grafting densities. The dependence on n_s is well approximated by an exponential decay at all grafting densities. Coherently with the qualitative observations derived from the z chain-end and tilt angle distributions, the reorientational dynamics of long terminal segments, $n_s \simeq 70$, is characterized by relaxation times of the order of microseconds for the highest grafting density considered, while decreases by more than an order of magnitude for the lowest one.

The relaxation times of the stiff, grafted segments of the polymer chains provide us with different information concerning the scaling of the brush properties with grafting densities. In this case, we use a different threshold, 0.9, to evaluate the relaxation time of the grafted segments from their rotational autocorrelation function. Indeed, their relaxation is much slower than for the terminal, mobile segments. Relaxation times are plotted as a function of n_s in the bottom panel of Figure 11. Again, relaxation times span 2 orders of magnitude going from the lowest to the highest grafting density. At all densities, τ_r first increases nearly exponentially with the length of the grafted segment. For the lowest density brush, this trend can be observed until $n_s = 110$, when τ_r decreases due to the high mobility of the upper monomers, which compensates for the overall elongation of the grafted segment. The change of slope of τ_r vs n_s is instead quite abrupt for the highest density brush, whose relaxation time sets to a plateau value in the range $70 < n_s < 110$, before starting to decrease.

DISCUSSION AND CONCLUSIONS

We have presented a computational study of PS brushes in a regime of high grafting density. This work relies on a new coarse-grained model of PS, based on the MARTINI coarse-grained force field. The model is chemically specific and allows for the simulation of polystyrene in different solvent environments. Here we focused on benzene, a good solvent for PS. The model is also computationally efficient, as MD simulations can be run with a time step of 20 fs, allowing the investigation of the system over time scales of tens of microseconds.

We can compare the outcomes of our simulations to those of previous computational works that used chemically nonspecific

dx.doi.org/10.1021/ma201980k |*Macromolecules* 2012, 45, 563–571

coarse-grained models. In terms of grafting density, we can translate our grafting densities into dimensionless grafting densities, $\sigma = Np^2/A$, p being the characteristic segment length of the polymer, N the number of monomers in the chains, and A the substrate area. p is the Kuhn length of the polymer, namely twice its persistence length; that for our PS model is 1 nm (in good agreement with experimental[31] and computational[45,46] data). Our numerical grafting densities can be thus converted in dimensionless grafting densities and result as $\sigma = 0.60$, 0.92, and 1.24.

Coluzza and Hansen[42] have identified three density regimes: for $\sigma < 0.004$, the brush is in the mushroom regime. For $0.01 < \sigma < 0.05$ the brush obeys the scaling behavior predicted by the self-consistent field (SCF) theory (that points to parabolic monomer density profiles). For $\sigma > 0.05$, the brush behavior deviates from the SFT predictions (and the density profiles flatten and stretch out). Clearly, all the brush densities analyzed here lay well within the high density, strong stretching regime. The density profile, far from being parabolic, is well fitted by a power law with exponent decreasing from 4.6 for the highest density brush to 4.2 for the lowest, as shown in Figure 12. The appearance of a small depletion layer for PS, close to the grafting surface, at the lowest grafting density analyzed here ($\sigma = 0.60$), is quantitatively coherent with the picture offered by Coluzza for $\sigma > 0.2$ and with other previous calculations.[32] The chain end distributions agree well with those shown by Coluzza as well. We remark that the shoulders in the averaged z profiles, resulting from single chains trapped in the brush bulk, are expected to be smoothed out on longer time scales and in larger samples.

The lateral pressure profiles do not show any change in sign at the top of the brush, consistently with the absence of a sharp polymer−solvent interface.[11] Nevertheless, they qualitatively change in the range of grafting densities considered, and for $\sigma = 1.24$ a well-defined plateau of the lateral pressure profile appears. At lower grafting densities, the interface extends all along the brush height, and the plateau disappears while the shape of the lateral pressure profiles approaches the one obtained by non-specific models at lower σ values.[11] Our results seem thus consistent with the results from chemically nonspecific calculations and allow for a quantitative estimation of the grafting density range corresponding to strong stretching for the specific case of polystyrene. It appears that the higher density brushes consist of a constant density and lateral pressure region close to the surface and a rather well-defined transition to the solvent region. The lower density system is one continuous transition, from the highest density/lateral pressure at the surface to the pure solvent.

Concerning the comparison with experiments, the density profiles emerging from our simulations closely resemble those observed by Devaux et al.,[33] which measured by neutron reflectivity the structure of PS brushes with $\sigma = 0.5$ and $N = 120$. The analysis of the experimental reflectivity spectra led to density profiles characterized by a clear plateau in the proximity of the grafting surface. Still, some discrepancies should be noted with the work by Ell et al.,[3] who synthesized polystyrene brushes by ATRP for which the grafting density was estimated to be 0.44 chains nm^{-2}. The molecular weight of the PS chains was again comparable with the one use in this study (15 kg/mol). Surprisingly, neutron reflectivity data suggest that the density profile of the polystyrene brush with $N = 150$ is well approximated by a power law decay with an exponent of 2.5, closer to the parabolic profile predicted by SCF theory than to the one provided by the best fit of our data (see Figure 12). One possible contribution to this discrepancy could

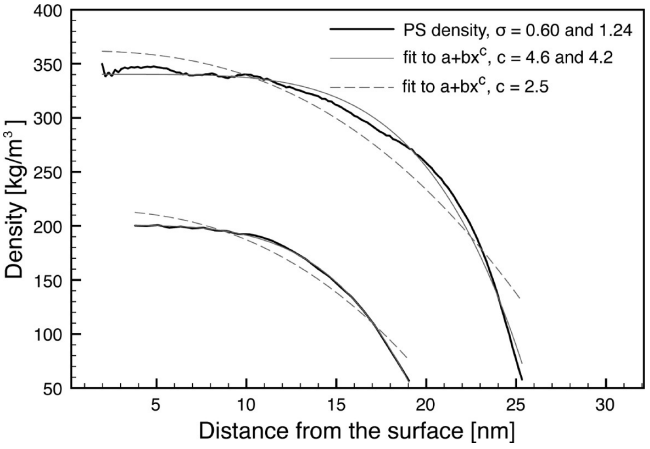

Figure 12. Density plot for polystyrene at the highest and lowest grafting densities considered in the paper. The exponential tails and the density oscillations close to the grafting surface are not included in the data sets. Thick gray lines correspond to the best power law fit, with exponent 4.6 and 4.2 for the $\sigma = 1.24$ and 0.60 grafting density, respectively. Dashed lines correspond to the best fit to power laws where the exponent was fixed to 2.5.

derive from the MARTINI model of benzene, which underestimates[16] the benzene density by a factor of 10%. Benzene molecules are thus effectively larger than they should be, and this might affect their penetration into the brush at the high brush densities considered here. We remark that when developing the MARTINI PS model,[22] the size of the beads composing the phenyl rings was tuned so as to reproduce with good accuracy the density of PS melts.

Our calculations show another interesting structural feature: the vertical alignment of the end points in the highly stretched configurations. The fully stretched configurations are rare events, and as such they do not stand out from average density plots or from the plot of the average order parameter, $P_2(\theta)$, as a function of the monomer index. But when $P_2(\theta)$ is plotted as a function of the distance from the surface, fully stretched configurations clearly appear to be characterized by the almost perfect alignment of the last bonds of the chain to the normal to the grafting surface. Such a feature had been predicted by SCF theory and reproduced by MD simulations,[47] though in a lower grafting density regime.

The analysis of average and single chain distributions of chain ends led to the identification of collapsed states, with the chain ends trapped inside the brush bulk. By looking at the time-dependent position of the chain ends, we could estimate life times of several microseconds for such trapped states. Our coarse-grained model has a relatively fine degree of coarse-graining, retaining the backbone−ring structure of polystyrene. This mapping is largely responsible for a limited acceleration of the dynamics with respect to atomistic simulations (chain diffusion coefficients in the melt differ from the atomistic ones by a factor of 3 at 400 K[22]). With this respect, our results concerning the dynamics of the brush can be considered to be quantitatively reliable.

The analysis of trapped states as varying the brush grafting densities shows that the transitions from collapsed to extended chain configurations become smoother and smoother as the grafting density is reduced. This is in agreement with our previous conclusions, pointing to the presence of an extended interface for the lowest grafting density brush and to a splitting into well-defined bulk and interface regions for the case of the highest density brush.

We identified two different relaxation regimes along the chain by splitting the chains in a grafted and a terminal part, represented by vectors connected to their grafted beads or chain ends, respectively, as shown in Figure 11. The relaxation time of the terminal, more mobile segments of the chains decays exponentially as the mobile segment length is progressively reduced. This trend is common to all the grafting densities considered. The dynamics of the grafted segment, on the contrary, depends qualitatively on the grafting density in the range analyzed. The relaxation time sets to a plateau value in an intermediate region of the brush, before dropping because of the increasing mobility of the terminal part of the chains. No such a plateau can be observed for the lowest grafting density considered in this study.

To conclude, we remark that the coarse-grained model we used, based on the MARTINI force field, was not developed with the explicit aim to deal with brush systems. Nevertheless, the overall good agreement between our findings and previous theoretical and experimental studies is promising. Our results validate the model for future use in the simulation of polymer-functionalized surfaces for both materials science and biological applications.

AUTHOR INFORMATION

Corresponding Author

*E-mail: giulia.rossi@inserm.fr (G.R.); rfaller@ucdavis.edu (R.F.).

Present Addresses

[⊥]INSERM UMR-S 665, 6, rue Alexandre Cabanel 75739 Paris Cedex 15, France.

ACKNOWLEDGMENT

R.F. thanks Aalto University for their kind hospitality during his visit. The authors thank Tonya L. Kuhl for interesting discussions and Jonathan Barnoud for developing a Gromacs tool for the order parameter analysis in a coarse-grained trajectory. The Davis part of this work was supported by the United States Department of Energy, Office of Science, Basic Energy Sciences, under Grant DE-FG02-06ER46340. This work has also been supported by the Academy of Finland through its COMP CoE grant. Computer time at CSC is also gratefully acknowledged.

REFERENCES

(1) Advincula, R. C.; Brittain, W. J.; Caster, K. C.; Ruhe, J. *Polymer Brushes*; Wiley-VCH: Weinheim, Germany, 2004.
(2) Lego, B.; François, M.; Skene, W. G.; Giasson, S. *Langmuir* **2009**, *25*, 5313.
(3) Ell, J. R.; Mulder, D. E.; Faller, R.; Patten, T. E.; Kuhl, T. L. *Macromolecules* **2009**, *42*, 9523–9527.
(4) Edmondson, S.; Osborne, V. L.; Huck, W. T. S. *Chem. Soc. Rev.* **2004**, *33*, 14–22.
(5) Landherr, L. J. T.; Cohen, C.; Agarwal, P.; Archer, L. A. *Langmuir* **2011**, *27*, 9387.
(6) Jhaveri, S. B.; Beinhoff, M.; Hawker, C. J.; Carter, K. R.; Sogah, D. Y. *ACS Nano* **2008**, *2*, 719.
(7) Diamanti, S.; Arifuzzaman, S.; Elsen, A.; Genzer, J.; Vaia, R. A. *Polymer* **2008**, *49*, 3770.
(8) Daoulas, K. C.; Terzis, A. F.; Mavrantzas, V. G. *J. Chem. Phys.* **2002**, *116*, 11028–11038.
(9) Zheng, J.; Li, L.; Chen, S.; Jiang, S. *Langmuir* **2004**, *20*, 8931–8938.
(10) Träskelin, P.; Kuhl, T. L.; Faller, R. *Phys. Chem. Chem. Phys.* **2009**, 11324–11332.
(11) Dimitrov, D. I.; Milchev, A.; Binder, K. *J. Chem. Phys.* **2007**, *127*, 084905.
(12) Binder, K. *Eur. Phys. J. E* **2001**, *9*, 293.
(13) Cordeiro, R. M.; Zschunke, F.; Müller-Plathe, F. *Macromolecules* **2010**, *43*, 1583–1591.
(14) Farah, K.; Leroy, F.; Müller-Plathe, F.; Bohm, M. C. *J. Phys. Chem. C* **2011**.
(15) Marrink, S.-J.; de Vries, A. H.; Mark, A. E. *J. Phys. Chem. B* **2004**, *108*, 750.
(16) Marrink, S.-J.; Risselada, H. J.; Yefimov, S.; Tieleman, D. P.; de Vries, A. H. *J. Phys. Chem. B* **2007**, *111*, 7812.
(17) Monticelli, L.; Kandasamy, S. K.; Periole, X.; Larson, R. G.; Tieleman, D. P.; Marrink, S.-J. *J. Chem. Theory Comput.* **2008**, *4*, 819.
(18) Vuorela, T.; Catte, A.; Niemelä, P. S.; Hall, A.; Hyvönen, M. T.; Marrink, S. J.; Karttunen, M.; Vattulainen, I. *PLoS Comput. Biol.* **2010**, *6*, e1000964.
(19) Catte, A.; Vuorela, T.; Niemelä, P.; Murtola, T.; Segrest, J. P.; Marrink, S. J.; Karttunen, M.; Vattulainen, I. *Biophys. J.* **2008**, *94*, 983.
(20) López, C. A.; Rzepiela, A. J.; de Vries, A. H.; Dijkhuizen, L.; Hünenberger, P. H.; Marrink, S. J. *J. Chem. Theor. Chem* **2009**, *5*, 3195.
(21) Wong-ekkabut, J.; Baoukina, S.; Triampo, W.; Tang, I.-M.; Tieleman, D. P.; Monticelli, L. *Nature Nanotechnol.* **2008**, *3*, 363.
(22) Rossi, G.; Monticelli, L.; Puisto, S. R.; Vattulainen, I.; Ala-Nissila, T. *Soft Matter* **2011**, *7*, 698.
(23) Lee, H.; de Vries, A. H.; Marrink, S.-J.; Pastor, R. W. *J. Phys. Chem. B* **2009**, *113*, 13186.
(24) Lee, H.; Larson, R. G. *J. Phys. Chem. B* **2008**, *112*, 7778–7784.
(25) Rossi, G.; Giannakopoulos, I.; Monticelli, L.; Rostedt, N. K. J.; Puisto, S. R.; Lowe, C.; Taylor, A. C.; Vattulainen, I.; Ala-Nissila, T. *Macromolecules* **2011**, DOI: 10.1021/ma200788.
(26) Milani, A.; Casalegno, M.; Castiglioni, C.; Raos, G. *Macromol. Theory Simul.* **2011**, *20*, 305.
(27) Gautieri, A.; Vesentini, S.; Redaelli, A. *J. Mol. Model.* **2010**, *16*, 1845.
(28) Ahmad, S.; Johnston, B. F.; Mackay, S. P.; Schatzlein, A. G.; Gellert, P.; Sengupta, D.; Uchegbu, I. F. *J. R. Soc., Interface* **2010**, *7*, S423.
(29) http://md.chem.rug.nl/cgmartini.
(30) Doi, M.; Edwards, S. F. *The Theory of Polymer Dynamics*; Clarendon Press: Oxford, 1986; Vol. 73.
(31) Cotton, J. P.; Decker, D.; Benoit, H.; Farnoux, B.; Higgins, J.; Jannink, G.; Ober, R.; Picot, C.; des Cloizeaux, J. *Macromolecules* **1974**, *7*, 863.
(32) Elliott, I. G.; Kuhl, T. L.; Faller, R. *Macromolecules* **2010**, *43*, 9131–9138.
(33) Devaux, C.; Cousin, F.; Beyou, E.; Chapel, J.-P. *Macromolecules* **2005**, *38*, 4296.
(34) Hess, B.; Kutzner, C.; van der Spoel, D.; Lindahl, E. *J. Chem. Theor. Comput.* **2008**, *4*, 435.
(35) Berendsen, H. J. C.; Postma, J. P. M.; van Gunsteren, W. F.; DiNola, A.; Haak, J. R. *J. Chem. Phys.* **1984**, *81*, 3684.
(36) Nosé, S. *Mol. Phys.* **1984**, *52*, 255–268.
(37) Hoover, W. G. *Phys. Rev. A* **1985**, *31*, 1695–1697.
(38) Nosé, S.; Klein, M. L. *Mol. Phys.* **1983**, *50*, 1055–1076.
(39) Parrinello, M. *J. Appl. Phys.* **1981**, *52*, 7182–7190.
(40) Israelachvili, J. N. *Surf. Sci. Rep.* **1992**, *14*, 109.
(41) Gao, J.; Luedtke, W. D.; Landman, U. *Phys. Rev. Lett.* **1997**, *79*, 705.
(42) Coluzza, I.; Hansen, J.-P. *Phys. Rev. Lett.* **2008**, *100*, 1.
(43) Elliott, I. G.; Mulder, D. E.; Traskelin, P. T.; Ell, J. R.; Patten, T. E.; Kuhl, T. L.; Faller, R. *Soft Matter* **2009**, *5*, 4612–4622.
(44) Ollila, O. H. S.; Risselada, H. J.; Louhivuori, M.; Lindahl, E.; Vattulainen, I.; Marrink, S. J. *Phys. Rev. Lett.* **2009**, *102*, 078101.
(45) Sun, Q.; Faller, R. *Macromolecules* **2006**, *39*, 812.
(46) Milano, G.; Müller-Plathe *J. Phys. Chem. B* **2005**, *39*, 18609.
(47) Seidel, C.; Netz, R. R. *Macromolecules* **2000**, *33*, 634.